Numerical Method for Analyzing Shielding Current Density in HTS Film with Multiple-Layer/Multiply-Connected Structure*)

Atsushi KAMITANI, Teruou TAKAYAMA, Soichiro IKUNO[1)] and Hiroaki NAKAMURA[2)]

Yamagata University, Yamagata 992-8510, Japan
[1)]*Tokyo University of Technology, Tokyo 192-0982, Japan*
[2)]*National Institute for Fusion Science, Gifu 509-5292, Japan*

(Received 22 November 2012 / Accepted 26 April 2013)

The governing equations of the shielding current density $\boldsymbol{j}$ in a high-temperature superconducting film are formulated for the case where the film contains cracks or holes. Since the derived equations cannot be solved only with the boundary condition $\boldsymbol{j} \cdot \boldsymbol{n} = 0$ on the film surface, additional conditions are also derived. A numerical method is proposed for solving the initial-boundary-value problem of the equations and its performance is evaluated by means of the numerical simulation of the permanent magnet method.

Keywords: critical current density, finite element method, high-temperature superconductor, integrodifferential equation, Newton method

DOI: 10.1585/pfr.8.2405078

1. Introduction

Recently, high-temperature superconductors (HTSs) have been proposed for numerous engineering applications: fusion magnet, energy storage system, power cable and magnetic shielding apparatus. Since the evaluation of the shielding current density is often required for the design of engineering applications, several numerical methods [1–3] have been so far proposed to calculate the shielding current density.

By assuming the thin-plate approximation, Yoshida *et al.* [1] derived the governing equation of the shielding current density in an HTS film. However, the resulting equation contains z (a coordinate in the thickness direction) as a parameter so that its solution has z-dependence. In contrast, the solution is assumed not to depend on z in the thin-plate approximation. For the purpose of resolving this contradiction, the authors averaged Faraday's law over the thickness to reformulate the governing equation of the shielding current density [2]. However, the obtained equation holds only for the an HTS film containing neither cracks nor holes.

The purpose of the present study is to derive the governing equations of the shielding current density in a multiple-layer HTS film with defects such as cracks and holes. Furthermore, a numerical method is developed for solving the initial-boundary-value problem of the equations and its performance is evaluated by means of numerical experiments.

2. Governing Equations

In this section, we derive the governing equations of the shielding current density in a multiple-layer HTS film containing cracks or holes. An HTS film of thickness b is exposed to the time-dependent magnetic field $\boldsymbol{B}/\mu_0$. Let us first assume that its cross section Ω vertical to the thickness direction does not change at all through the thickness (see Fig. 1). The cross section Ω is simply connected for an HTS film containing no defects, whereas it is multiply connected for an HTS film with cracks or holes. If Ω is multiply connected, its boundary $\partial\Omega$ is composed of not only the outer boundary C_0 but the inner boundaries, $C_1, C_2, \cdots, C_K$. In the following, the region enclosed by C_k and its area are denoted by Ω_k and A_k, respectively.

By taking the thickness direction as z-axis and choos-

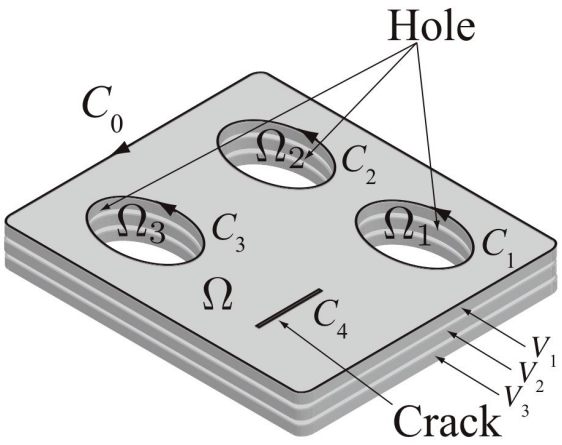

Fig. 1 A schematic view of an HTS film with multiple-layer and multiply-connected structure.

author's e-mail: kamitani@yz.yamagata-u.ac.jp
*) This article is based on the presentation at the 22nd International Toki Conference (ITC22).

ing the centroid of the HTS film as the origin, we use the Cartesian coordinate system $\langle O : \boldsymbol{e}_x, \boldsymbol{e}_y, \boldsymbol{e}_z \rangle$. In the following, $\boldsymbol{x}$ and $\boldsymbol{x}'$ are position vectors of two points in the xy plane, whereas z and z' are defined by $\boldsymbol{z} = \boldsymbol{x} + z\boldsymbol{e}_z$ and $\boldsymbol{z}' = \boldsymbol{x}' + z'\boldsymbol{e}_z$, respectively. In addition, $\boldsymbol{l}$ and $\boldsymbol{n}$ denote a tangent unit vector and a normal unit vector on $\partial\Omega$, respectively.

2.1 Multiple thin-layer approximation

In general, HTS films have a strong anisotropy in the critical current density [1]: its component along the c-axis is negligibly small as compared with that parallel to the a-b plane. In order to take the anisotropy into account, we set the following two assumptions:

1. An HTS film has an M-layered structure and the shielding current density never flows across the interface between every two adjacent layers.
2. Each layer is sufficiently thin that both the shielding current density and the electric field may not change in the thickness direction.

The above assumptions are called a multiple-thin-layer approximation [2]. In the following, the pth layer and its boundary are denoted by V_p and ∂V_p, respectively. In addition, the shielding current density and the electric field in V_p are denoted by $\boldsymbol{j}_p$ and $\boldsymbol{E}_p$, respectively, and the magnetic flux density generated by $\boldsymbol{j}_p$ is denoted by $\boldsymbol{B}_p$.

Under the above assumptions, the behavior of the electromagnetic fields can be expressed as

$$\frac{\partial}{\partial t}\sum_{q=1}^{M}\langle \boldsymbol{e}_z \cdot \boldsymbol{B}_q \rangle_p + \boldsymbol{e}_z \cdot (\nabla \times \boldsymbol{E}_p) + \frac{\partial}{\partial t}\langle \boldsymbol{e}_z \cdot \boldsymbol{B} \rangle_p = 0 \quad (p = 1, 2, \cdots, K), \tag{1}$$

$$\boldsymbol{B}_q = \mu_0 \nabla \times \iiint_{V_q} w^*(\boldsymbol{z}, \boldsymbol{z}')\boldsymbol{j}_q(\boldsymbol{x}', t)\,\mathrm{d}^3\boldsymbol{z}' \quad (q = 1, 2, \cdots, K), \tag{2}$$

where $w^*(\boldsymbol{z}, \boldsymbol{z}') = (4\pi|\boldsymbol{z} - \boldsymbol{z}'|)^{-1}$. In addition, the square bracket $\langle\ \rangle_p$ means an average operator over the thickness of V_p.

In HTS films, $\boldsymbol{E}_p$ and $\boldsymbol{j}_p$ are closely related to each other through the J-E constitutive equation. For the equation, we adopt the following power law [4–7]:

$$\boldsymbol{E}_p = E(|\boldsymbol{j}_p|)\frac{\boldsymbol{j}_p}{|\boldsymbol{j}_p|}, \quad E(j) = E_{\mathrm{C}}\left(\frac{j}{j_{\mathrm{C}}}\right)^N, \tag{3}$$

where j_{C} and E_{C} denote the critical current density and the critical electric field, respectively, and N is a positive constant.

As usual, the initial and boundary conditions are assumed as

$$\boldsymbol{j}_p = \boldsymbol{0} \quad \text{at } t = 0 \quad (p = 1, 2, \cdots, K), \tag{4}$$

$$\boldsymbol{j}_p \cdot \boldsymbol{n} = 0 \quad \text{on } \partial V_p \quad (p = 1, 2, \cdots, K). \tag{5}$$

By solving the initial-boundary-value problem of (1) and (2), we can analyze the time evolution of the shielding current density.

2.2 Current vector potential

Under the multiple-thin-layer approximation, there exists a scalar function $S_q(\boldsymbol{x}, t)$ such that

$$\boldsymbol{j}_q = \nabla \times [(S_q/\epsilon)\,\boldsymbol{e}_z], \tag{6}$$

where $\epsilon \equiv b/(2M)$. Hence, the electromagnetic state of the HTS film is characterized by the following M-dimensional vector-valued function:

$$\overrightarrow{S}(\boldsymbol{x}, t) = \sum_{p=1}^{M}\overrightarrow{e_p}\,S_p(\boldsymbol{x}, t).$$

Here, $\{\overrightarrow{e_1}, \overrightarrow{e_2}, \cdots, \overrightarrow{e_M}\}$ are the orthonormal system of the M-dimensional vector space. Incidentally, as is apparent from (6), $(S_q/\epsilon)\,\boldsymbol{e}_z$ is a current vector potential of $\boldsymbol{j}_q$.

In terms of $\overrightarrow{S}$, the initial and boundary conditions, (4) and (5), can be written in the form,

$$\overrightarrow{S} = \overrightarrow{0} \text{ at } t = 0, \tag{7}$$

$$\overrightarrow{S} = \overrightarrow{0} \text{ on } C_0, \tag{8}$$

$$\overrightarrow{S} = \overrightarrow{S_k}(t) \text{ on } C_k \quad (k = 1, 2, \cdots, K), \tag{9}$$

where $\overrightarrow{S_k}(t)$'s are unknown vector-valued functions of time. Note that additional conditions are required for determining $\overrightarrow{S_k}(t)$'s.

Next, we derive the governing equation of $\overrightarrow{S}$. Substitution of (6) into (2) yields

$$\begin{aligned}\frac{1}{\mu_0}\sum_{p=1}^{M}\overrightarrow{e_p}\,\langle \boldsymbol{e}_z \cdot \boldsymbol{B}_q \rangle_p &= \frac{1}{\epsilon}\left(\overrightarrow{e_q} \otimes \overrightarrow{e_q}\right) \cdot \left[c(\boldsymbol{x})\,\overrightarrow{S}(\boldsymbol{x}, t) + \sum_{l=1}^{K} c_l(\boldsymbol{x})\,\overrightarrow{S_l}(t)\right] \\ &\quad + \iint_{\Omega} \overleftrightarrow{Q}(|\boldsymbol{x} - \boldsymbol{x}'|) \cdot \overrightarrow{S}(\boldsymbol{x}', t)\,\mathrm{d}^2\boldsymbol{x}' \\ &\quad + \sum_{l=1}^{K}\iint_{\Omega_l} \overleftrightarrow{Q}(|\boldsymbol{x} - \boldsymbol{x}'|)\,\mathrm{d}^2\boldsymbol{x}' \cdot \overrightarrow{S_l}(t),\end{aligned} \tag{10}$$

where $c(\boldsymbol{x})$ and $c_l(\boldsymbol{x})$ are the shape coefficient associated with Ω and that with Ω_l, respectively. In addition, $\overleftrightarrow{Q}(r)$ is the second-order tensor whose (p, q) element $Q_{pq}(r)$ is given in [2]. By substituting (10) into (1), we get the following integrodifferential equation:

$$\mu_0\frac{\partial}{\partial t}(\hat{W}\overrightarrow{S}) + \overrightarrow{E}(\overrightarrow{S}) + \frac{\partial\overrightarrow{\beta}}{\partial t} = \overrightarrow{0} \text{ in } \Omega. \tag{11}$$

Here, M-dimensional vectors, $\overrightarrow{E}(\overrightarrow{S})$ and $\overrightarrow{\beta}$, are given by

$$\overrightarrow{E}(\overrightarrow{S}) = \sum_{p=1}^{M} \overrightarrow{e_p}\,[\boldsymbol{e}_z \cdot (\nabla \times \boldsymbol{E}_p)],$$

$$\overrightarrow{\beta} = \sum_{p=1}^{M} \overrightarrow{e_p}\,\langle \boldsymbol{e}_z \cdot \boldsymbol{B}\rangle_p,$$

and $\hat{W}$ is a linear operator defined by

$$\hat{W}\overrightarrow{S} \equiv \frac{1}{\epsilon}\overrightarrow{S} + \iint_{\Omega} \overleftrightarrow{Q}(|\boldsymbol{x}-\boldsymbol{x}'|)\cdot\overrightarrow{S}(\boldsymbol{x}',t)\,\mathrm{d}^2\boldsymbol{x}' + \sum_{l=1}^{K}\iint_{\Omega_l}\overleftrightarrow{Q}(|\boldsymbol{x}-\boldsymbol{x}'|)\,\mathrm{d}^2\boldsymbol{x}'\cdot\overrightarrow{S_l}(t).$$

As mentioned above, additional conditions must be imposed to determine $\overrightarrow{S_k}(t)$ $(k = 1, 2, \cdots, K)$. For the conditions, the integral forms of Faraday's law on Ω_k's are adopted. By rewriting them in terms of $\overrightarrow{S}$, we get

$$\mu_0 \frac{\mathrm{d}}{\mathrm{d}t}\overrightarrow{\omega_k}[\overrightarrow{S}] + \overrightarrow{\varphi_k}(\overrightarrow{S}) + \frac{\mathrm{d}\overrightarrow{\Phi_k}}{\mathrm{d}t} = \overrightarrow{0}. \tag{12}$$

Here, the functional $\overrightarrow{\omega_k}[\overrightarrow{S}]$ is defined by

$$\overrightarrow{\omega_k}[\overrightarrow{S}] \equiv \frac{A_k}{\epsilon}\overrightarrow{S} + \iint_{\Omega_k}\mathrm{d}^2\boldsymbol{x}\iint_{\Omega}\overleftrightarrow{Q}(|\boldsymbol{x}-\boldsymbol{x}'|)\cdot\overrightarrow{S}(\boldsymbol{x}',t)\,\mathrm{d}^2\boldsymbol{x}' + \sum_{l=1}^{K}\iint_{\Omega_k}\mathrm{d}^2\boldsymbol{x}\iint_{\Omega_l}\overleftrightarrow{Q}(|\boldsymbol{x}-\boldsymbol{x}'|)\,\mathrm{d}^2\boldsymbol{x}'\cdot\overrightarrow{S_l}(t).$$

In addition, $\overrightarrow{\varphi_k}(\overrightarrow{S})$ and $\overrightarrow{\Phi_k}$ are given by

$$\overrightarrow{\varphi_k}(\overrightarrow{S}) = \sum_{p=1}^{M}\overrightarrow{e_p}\oint_{C_k}\boldsymbol{E}_p\cdot\boldsymbol{l}\,\mathrm{d}s,$$

$$\overrightarrow{\Phi_k} = \sum_{p=1}^{M}\overrightarrow{e_p}\iint_{\Omega_k}\langle\boldsymbol{e}_z\cdot\boldsymbol{B}\rangle_p\,\mathrm{d}^2\boldsymbol{x},$$

where s denotes an arclength along C_k. Consequently, (8), (9) and (12) are the boundary conditions to (11), whereas (7) is the initial condition to (11). If the initial-boundary-value problem of (11) is solved, the time variation of the shielding current density is determined.

3. Virtual Voltage Method

In this section, the numerical method for solving the initial-boundary-value problem of (11) is described in detail. In the following, the superscript (n) denotes a value at time $t = n\Delta t$, where Δt is a time-step size.

If the initial-boundary-value problem of (11) is discretized with the backward Euler method, $\overrightarrow{S}^{(n)}$ becomes a solution of the following nonlinear boundary-value problem:

$$\overrightarrow{G}(\overrightarrow{S}) \equiv \mu_0\hat{W}\overrightarrow{S} + \Delta t\,\overrightarrow{E}(\overrightarrow{S}) - \overrightarrow{u} = \overrightarrow{0} \text{ in } \Omega, \tag{13}$$

$$\overrightarrow{S} \in H(\bar{\Omega}), \tag{14}$$

$$\overrightarrow{\gamma_k}[\overrightarrow{S}] \equiv \mu_0\overrightarrow{\omega_k}[\overrightarrow{S}] + \Delta t\,\overrightarrow{\varphi_k}(\overrightarrow{S}) - \overrightarrow{v_k} = \overrightarrow{0} \quad (k = 1, 2, \cdots, K), \tag{15}$$

Here, $\overrightarrow{u}$ and $\overrightarrow{v_k}$ are given by

$$\overrightarrow{u} = \mu_0\hat{W}\overrightarrow{S}^{(n-1)} - (\overrightarrow{\beta}^{(n)} - \overrightarrow{\beta}^{(n-1)}),$$

$$\overrightarrow{v_k} = \mu_0\overrightarrow{\omega_k}[\overrightarrow{S}^{(n-1)}] - (\overrightarrow{\Phi_k}^{(n)} - \overrightarrow{\Phi_k}^{(n-1)}).$$

In addition, the function space $H(\bar{\Omega})$ is defined by

$$H(\bar{\Omega}) \equiv \left\{\overrightarrow{w}(\boldsymbol{x}) : \overrightarrow{w} = \overrightarrow{0} \text{ on } C_0,\ \frac{\partial\overrightarrow{w}}{\partial s} = \overrightarrow{0} \text{ on } C_k\ (k = 1, 2, \cdots, K)\right\}.$$

After a straightforward calculation, we can get the weak form that is equivalent to (13) and (15). It must be noted here that the derived weak form completely includes the boundary condition (15). In other words, (15) is treated as a natural boundary condition. Therefore, the numerically evaluated value $\overrightarrow{N_k}[\overrightarrow{S}]$ of $\overrightarrow{\gamma_k}[\overrightarrow{S}]$ does not always vanish. In fact, the results of computations show that these tendencies become remarkable with a decrease in b. Throughout the present paper, the method, in which (15) is treated as a natural boundary condition, is called the conventional method.

In order to suppress the numerical error in $\overrightarrow{N_k}[\overrightarrow{S}]$, we propose the virtual voltage method [7]. The basic idea of this method is to apply the virtual voltage ϕ_k^p along the inner boundary C_k of V_p so as to have $\overrightarrow{N_k}[\overrightarrow{S}] = \overrightarrow{0}$ strictly fulfilled. Specifically, the boundary condition (15) is replaced with the following two conditions:

$$\frac{\overrightarrow{\gamma_k}[\overrightarrow{S}]}{\Delta t} = \sum_{p=1}^{M}\overrightarrow{e_p}\phi_k^p \equiv \overrightarrow{\phi_k} \quad (k = 1, 2, \cdots, K), \tag{16}$$

$$\overrightarrow{N_k}[\overrightarrow{S}] = \overrightarrow{0} \quad (k = 1, 2, \cdots, K), \tag{17}$$

where ϕ_k^p's are all unknown constants. As a result, the nonlinear boundary-value problem is modified so as to be composed of (13), (14), (16) and (17). The modified nonlinear problem is numerically solved for $\overrightarrow{S}$ and $\{\overrightarrow{\phi_k}\}_{k=1}^{K}$.

The Newton method is applied to the modified nonlinear problem. In the Newton method, the numerical solution $\overrightarrow{S}$ is iteratively determined by using the following two steps.

1. The linear boundary-value problem:

$$\delta\overrightarrow{G} = -\overrightarrow{G}(\overrightarrow{S}) \text{ in } \Omega,$$
$$\delta\overrightarrow{S} \in H(\bar{\Omega}),$$
$$\delta\overrightarrow{\gamma_k} - \Delta t\,\delta\overrightarrow{\phi_k} = -(\overrightarrow{\gamma_k}[\overrightarrow{S}] - \Delta t\,\overrightarrow{\phi_k}),$$
$$\delta\overrightarrow{N_k} = -\overrightarrow{N_k}[\overrightarrow{S}],$$

   is solved for the corrections, $\delta\overrightarrow{S}$ and $\{\delta\overrightarrow{\phi_k}\}_{k=1}^{K}$.

2. The approximate solutions, $\overrightarrow{S}$ and $\{\overrightarrow{\phi_k}\}_{k=1}^{K}$, are updated by

$$\overrightarrow{S} := \overrightarrow{S} + \delta\overrightarrow{S},$$
$$\overrightarrow{\phi_k} := \overrightarrow{\phi_k} + \delta\overrightarrow{\phi_k}\ (k = 1, 2, \cdots, K).$$

Here, $\delta\vec{G}$, $\delta\vec{\gamma_k}$ and $\delta\vec{N_k}$ are Fréchet derivatives of $\vec{G}(\vec{S})$, $\vec{\gamma_k}[\vec{S}]$ and $\vec{N_k}[\vec{S}]$, respectively. The above two steps are repeated until both $\|\delta\vec{S}\|/\|\vec{S}\|$ and $\max_{k=1}^{K}\|\delta\vec{\phi_k}\|/\|\vec{\phi_k}\|$ become negligibly small. Incidentally, the linear boundary-value problem is solved with the finite element method.

4. Numerical Experiments

By using the virtual voltage method, a numerical code has been developed for analyzing the time evolution of the shielding current density. In this section, we evaluate the performance of the virtual voltage method by means of the code. To this end, the numerical simulation of the permanent magnet (PM) method [8, 9] is performed by means of the code.

4.1 PM method

The PM method is one of the contactless methods for measuring j_C. In the method, a cylindrical PM of radius R and height H is placed above an HTS film so that the symmetry axis of the magnet may be vertical to the film surface. The magnet is first brought closer to the film and it is subsequently moved away from the film. During the movement of the magnet, the electromagnetic force F_z acting on the film is measured.

In the PM method, the distance L between the magnet bottom and the film surface is controlled as follows: it is first reduced from $L = L_{\max}$ to $L = L_{\min}$ at a constant speed $v = (L_{\max} - L_{\min})/\tau_0$ and, just after that, it is increased back to $L = L_{\max}$ at the same speed.

Throughout the present study, an HTS film is assumed to have a square cross section of side length a. Furthermore, it is assumed to contain a crack whose cross section is a line segment connecting two points, $(0, \pm L_c/2)$, in the xy plane. In the following, the geometrical and physical parameters are fixed as follows: $a = 40\,\text{mm}$, $j_C = 2\,\text{MA/cm}^2$, $E_C = 0.1\,\text{mV/m}$, $N = 20$, $L_{\max} = 20\,\text{mm}$, $L_{\min} = 0.5\,\text{mm}$, $\tau_0 = 39\,\text{s}$, $R = 2.5\,\text{mm}$, $H = 3.0\,\text{mm}$, $B_F = 0.3\,\text{T}$, and $(x_{PM}, y_{PM}) = (0\,\text{mm}, 0\,\text{mm})$. Here, the symmetry axis of the PM is denoted by $(x, y) = (x_{PM}, y_{PM})$. In addition, B_F is the magnitude of the magnetic flux density at $(x, y, z) = (x_{PM}, y_{PM}, b/2)$ for $L = L_{\min}$ and it is adopted as the measure of the intensity of the PM.

4.2 Performance of proposed method

Let us first compare the performance of the proposed method with that of the conventional method. To this end, the PM method is numerically reproduced for the case with $(x_c, y_c) = (0\,\text{mm}, 0\,\text{mm})$, $L_c = 32\,\text{mm}$, $b = 200\,\text{nm}$ and $M = 1$. By using the two methods, the values $S_1(C_1)$ of the scalar function S_1 on the crack surface are calculated as functions of time. The results of computations are plotted in Fig. 2. This figure indicates that, for $t/\tau_0 \lesssim 0.25$, the calculated values by the two methods are in reasonable agreement with each other. In contrast, for $t/\tau_0 \gtrsim 0.25$, the calculated values by the conventional method begin to deviate from those by the proposed method. This result suggests that, as time advances, the numerical solutions by the two methods will become totally different. In fact, the $\boldsymbol{j}$-distributions by the two methods show widely different patterns (see Figs. 3 (a) and 3 (b)).

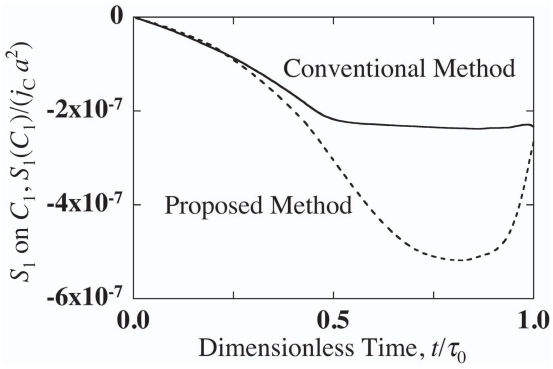

Fig. 2 The time dependence of the value of S_1 on the crack surface C_1.

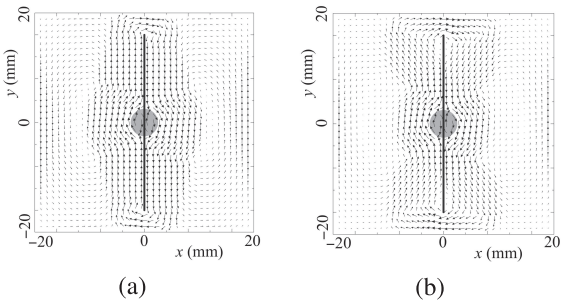

Fig. 3 Spatial distributions of the shielding current density $\boldsymbol{j}$ at $t = \tau_0$. Here, the $\boldsymbol{j}$-distribution is determined by using (a) the conventional method and (b) the proposed method. In both figures, cracks are denoted by thick line segments.

Next, we investigate the influence of the multiple-layer structure on the electromagnetic force F_z. To this end, F_z-L curves are numerically determined for various values of M and are depicted in Figs. 4 (a) and 4 (b). For the case with $b = 1\,\mu\text{m}$, F_z-L curves are not at all influenced by the number M of layers. On the other hand, the value of F_z depends strongly on M for the case with $b = 1\,\text{mm}$. This result indicates that the multiple-layer structure is indispensable for calculating the shielding current density in an HTS bulk.

5. Conclusion

We have formulated an initial-boundary-value problem of the shielding current density in an HTS film with a multiple-layer and multiply-connected structure. In addition, we have proposed a numerical method for accurately solving the problem. On the basis of the proposed method, a numerical code has been developed for analyzing the time evolution of the shielding current density. By using the code, the performance of the proposed method is

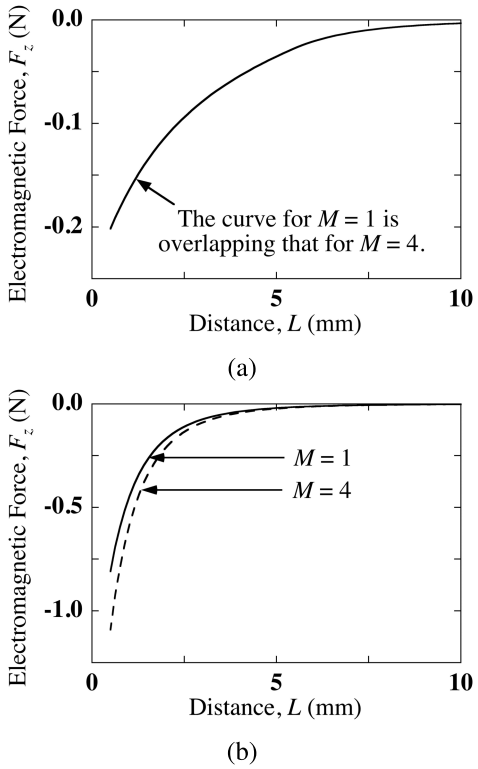

Fig. 4 The electromagnetic force F_z as functions of the magnet-film distance L for the case with (a) b = 1 μm and for the case with (b) b = 1 mm. Here, an HTS sample is assumed to contain neither cracks nor holes.

compared with that of the conventional method.

Conclusions obtained in the present study are summarized as follows.

1. As time advances, a numerical solution by the conventional method will deviate from that by the proposed method. This deviation is attributable to the fact that the integral form of Faraday's law is not exactly satisfied in the conventional method. In this sense, if an HTS film contains cracks/holes, not the conventional method but the proposed method should be applied to the shielding current analysis in the film.
2. A numerical solution for an HTS film is hardly affected by the number of layers, whereas that for an HTS bulk is very sensitive to the number of layers. Hence, the multiple-layer structure should be assumed in analyzing the shielding current density in an HTS bulk.

Acknowledgments

This work was supported in part by Japan Society for the Promotion of Science under a Grant-in-Aid for Scientific Research (C) No. 24560321. A part of this work was also performed with the support and under the auspices of the NIFS Collaboration Research program (NIFS11KNTS011, NIFS12KNXN237).

[1] Y. Yoshida, M. Uesaka and K. Miya, IEEE. Trans. Magn. **30**, 3503 (1994).
[2] A. Kamitani and S. Ohshima, IEICE Trans. Electron. **E82-C**, 766 (1999).
[3] M. Tsuchimoto and H. Kamijo, Physica C **463**, 1352 (2007).
[4] R. Fresa, G. Rubinacci, S. Ventre, F. Villone and W. Zamboni, IEEE. Trans. Magn. **45**, 988 (2009).
[5] G.P. Lousberg, J.F. Fagnard, M. Ausloos, P. Vanderbemden and B. Vanderheyden, IEEE Trans. Appl. Supercond. **20**, 33 (2010).
[6] A. Kamitani, T. Takayama and S. Ikuno, IEEE. Trans. Magn. **47**, 1138 (2011).
[7] A. Kamitani and T. Takayama, IEEE. Trans. Magn. **48**, 727 (2012).
[8] S. Ohshima, K. Takeishi, A. Saito, M. Mukaida, Y. Takano, T. Nakamura, T. Suzuki and M. Yokoo, IEEE Trans. Appl. Supercond. **15**, 2911 (2005).
[9] S. Ikuno, T. Takayama, A. Kamitani, K. Takeishi, A. Saito and S. Ohshima, IEEE Trans. Appl. Supercond. **19**, 3750 (2009).